JPE 18-1-17

https://doi.org/10.6113/JPE.2018.18.1.185
ISSN(Print): 1598-2092 / ISSN(Online): 2093-4718

Modal Analysis of Resonance and Stable Domain Calculation of Active Damping in Multi-inverter Grid-connected Systems

Jian Wu†, Tao Chen*, Wanqin Han*, Jiaqi Zhao*, Binbin Li*, and Dianguo Xu*

†,*School of Electrical Engineering and Automation, Harbin Institute of Technology, Harbin, China

Abstract

Interaction among multiple grid-connected inverters has a negative impact on the stable operations and power quality of a power grid. The interrelated influences of inverter inductor–capacitor–inductor filters constitute a high-order power network, and consequently, excite complex resonances at various frequencies. This study first establishes a micro-grid admittance matrix, in which inverters use deadbeat control. Multiple resonances can then be evaluated via modal analysis. For the active damping method applied to deadbeat control, the sampling frequency and the stable domain of the virtual damping ratio are also presented by analyzing system stability in the discrete domain. Simulation and experimental results confirm the efficiency of modal analysis and stable domain calculation in multi-inverter grid-connected systems.

Key words: Active damping, Deadbeat control, Inductor–capacitor–inductor (LCL) filter, Modal analysis, Stability, Parallel inverters, Resonant

I. INTRODUCTION

The utilization of renewable energy has been one of the most promising fields in the area of power systems in recent years. However, the stability of electric power systems has become a crucial issue and has attracted significant attention from utility operators and academic researchers due to the necessity of power converters for interfacing fluctuating resources [1]-[3]. Power converters produce discrete output waveforms with a considerable amount of harmonic components, which have to be mitigated by using passive filters interposed between the converter and the grid. In particular, the inductor–capacitor–inductor (LCL) filter has elicited significant research attention due to its good harmonics attenuation performance. The LCL filter has a steeper slope (60 dB/decade) than the single reactance L filter; hence, better attenuation to high-frequency components is achieved. However, if it is not designed and tuned well, the LCL filter can introduce a significant resonant peak, which can lead to serious stability problems due to different phase shifts or the amplification of intrinsically critical situations in a system with many distinct generators. Numerous studies have investigated passive and active damping for restraining resonance, but they have only focused on a single LCL inverter [4]-[7]. The resonance characteristic of multiple inverters clearly differs. The interrelated influences of paralled inverter LCL filters excite complex resonances at various frequencies and negatively impact the stable operation and power quality of power grids. Several methods for restraining LCL filter resonance in multi-inverter grid-connected systems, including open-loop pole-zero compensation, double-loop current control, and virtual-impedance, have been presented [8]-[11]. In [8], a simplified passive circuit model was proposed to investigate resonances without considering the influence of inverters. In [9], the interaction of multiple inverters based on the open-loop transfer function matrix was described, which showed that grid series impedance is equivalent to N times that of a single inverter. Reference [10] introduced a control system for the impedance modeling of a multi-inverter system and analyzed harmonic interaction between an inverter and a grid; however, it did not analyze interaction between inverters.

In [12], a current-controlled voltage-source inverter was

Manuscript received May 26, 2017; accepted Sep. 25, 2017
Recommended for publication by Associate Editor Jongbok Baek.
†Corresponding Author: wujianhit@hotmail.com
Tel: +86-0451-86413420, Fax: +86-0451-86413420,
*School of Electrical Eng. and Automation, Harbin Inst. of Tech., China

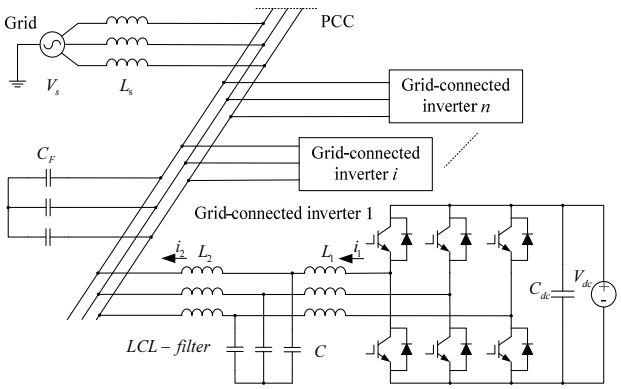

Fig. 1. Configuration of a multi-inverter grid-connected system.

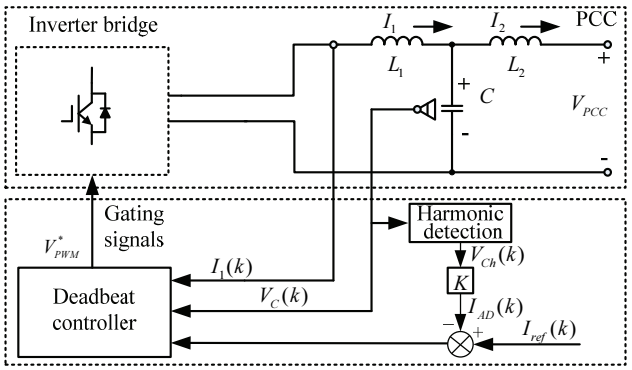

Fig. 2. Illustration of the deadbeat-controlled inverter system with active damping.

considered. The inverter, which is parallel with the output impedance, was introduced into the passive network model. Thus, the equivalent impedance model of multiple inverters was established. An interesting finding is that resonance peak changes with parallel sets; however, the Norton equivalent circuit is too complex for analyzing resonant characteristics [13]-[15].

Meanwhile, modal analysis methods have been reported effective for analyzing power system resonance [16]-[18]. They are suitable for evaluating micro-grid resonance and can obtain not only resonance frequency but also the extent of resonance based on the change in the network matrix characteristic root.

This study presents the multi-inverter grid-connected system impedance model and analyzes the resonant characteristics of the system using the modal analysis method. Furthermore, the stability domain of virtual damping resistance is analyzed, which shows the coupling relationships among sampling frequency, the virtual damping coefficient, and system parameters. The remainder of this paper is organized as follows. The modeling and control of multiple inverters are analyzed in Section II. The modal analysis of resonance and the z-domain stability of active damping based on parallel virtual resistance are discussed in Section III. In Section IV, the theoretical analysis is validated through experimental tests. Finally, analyses and conclusions are presented in Section V.

II. Modal Analysis of Multi-inverter Grid-connected System

This section analyzes the possible resonance phenomenon in a grid with multiple inverters, each with deadbeat current control. The configuration of this system is shown in Fig. 1. Each inverter is connected to the point of common coupling (PCC) though an LCL filter. L_1 is the inverter-side reactance, L_2 is the grid-side reactance, and C is the filter capacitance. Meanwhile, the grid reactance is L_s and the compensation capacitor is C_F. The schematic of a single equivalent system is further presented in Fig. 2, where I_1 is considered the current feedback by the deadbeat control and capacitor voltage V_c is measured for active damping.

As shown in Fig. 2, the harmonic capacitor voltage (V_{ch}) is separated using a harmonic detector, which is constructed based on instantaneous power theory in a rotating frame. The harmonic damping current can be described as

$$I_{AD}(k) = \frac{V_{ch}(k)}{K}, \tag{1}$$

where $1/K$ is the value of virtual damping resistance. With active damping, the deadbeat control is obtained as

$$V^*_{PWM}(k) = 1.5V_c(k) - 0.5V_c(k-1) + L_1 \frac{I_{ref}(k) + I_{AD}(k) - I_1(k)}{T_s}, \tag{2}$$

where T_s is the sampling period that corresponds to the switching period, $V^*_{PWM}(k)$ is the reference pulse-width modulation voltage of the k-th switching period. $I_{ref}(k)$ and $I_1(k)$ are the reference and measured inverter currents at the k-th period, respectively. $V_{ref}(k)$ and $V_{ref}(k-1)$ are the measured capacitor voltage at the k-th and $(k-1)$-th switching periods, respectively. When active damping is implemented in the deadbeat controller in Eq. (2), system performance will be similar to the case that uses passive damping only at the resonant frequency.

A. Closed-loop Multi-inverter Model

In this section, the closed-loop multi-inverter current source model of deadbeat current-controlled inverter systems is presented.

Fig. 3 illustrates the equivalent circuit of a single closed-loop inverter system. The inverter can be considered a current source due to the deadbeat control, and thus, Norton's equivalent circuit of a closed-loop inverter system is unnecessary. The complex resonances within a multi-inverter system can also be investigated based on this simple model. The equivalent circuit of a multi-inverter system is presented in Fig. 4, which can be obtained by replacing each inverter in Fig. 1 with a current source. The inverter-side reactor (L_1) can be disregarded due to the use of deadbeat current control, thereby reducing model complexity.

B. Modal Analysis of Multi-inverter System

When compensation capacitors are installed in the distribution power system, the resonance features of the multi-inverter grid-connected system will be more complex. Through the proposed simple model, the behavior of the multi-inverter grid-connected system can be described using an admittance matrix:

$$\mathbf{V} = \mathbf{Y}^{-1}\mathbf{I}, \tag{3}$$

$$Z\mathbf{I} = \mathbf{V}, \tag{4}$$

where $\mathbf{Y}$ and $\mathbf{Z}$ are the network admittance matrix and network impedance matrix, respectively. V is the nodal voltage, and I is the nodal injected current.

Resonance is related to the singularity of the inverted network admittance matrix. A singular Y matrix will occur only when one of the eigenvalues of the matrix is zero, which can be the real source of the resonance phenomenon. Consequently, the analysis of harmonic resonance can be transformed into the study of critical resonance modes.

A sharp harmonic resonance indicates that some nodal voltages are extremely high. This phenomenon will occur when the Y matrix approaches singularity. The matrix can be decomposed into the following:

$$\mathbf{Y} = \mathbf{L}\boldsymbol{\Lambda}\mathbf{T}, \tag{5}$$

where $\boldsymbol{\Lambda}$ is the diagonal eigenvalue matrix; L and T are the left and right eigenvector matrices, respectively; and $L = T^{-1}$.

When Eq. (5) is substituted into Eq. (3), the following is obtained:

$$\mathbf{TV} = \boldsymbol{\Lambda}^{-1}\mathbf{TI}. \tag{6}$$

When U = TV is defined as the modal voltage vector and J = TI as the modal current vector, Eq. (6) can be simplified as follows:

$$\begin{bmatrix} U_1 \\ U_2 \\ \vdots \\ U_n \end{bmatrix} = \begin{bmatrix} \lambda_1^{-1} & 0 & 0 & 0 \\ 0 & \lambda_2^{-1} & 0 & 0 \\ 0 & 0 & \cdots & 0 \\ 0 & 0 & 0 & \lambda_n^{-1} \end{bmatrix} \begin{bmatrix} J_1 \\ J_2 \\ \vdots \\ J_n \end{bmatrix}, \tag{7}$$

where λ_i is the eigenvalue and λ_i^{-1} is the modal impedance. Eq. (7) shows that if λ_i is extremely small or equal to zero, then a small injection of modal current J_i will lead to a large modal voltage U_i. That is, the location and frequency of resonance can be easily identified in the modal domain.

In Fig. 4, the multi-inverter grid-connected system is an (n+1) bus system, and its admittance matrix can be expressed as

$$Y = \begin{bmatrix} Y_S + Y_{CF} + nY_L & -Y_L & \cdots & -Y_L \\ -Y_L & Y_L + Y_C & 0 & \cdots \\ \cdots & 0 & \cdots & 0 \\ -Y_L & \underbrace{\cdots \quad 0 \quad Y_L + Y_C}_{n} & & \end{bmatrix} \Big\}\, n, \tag{8}$$

where $Y_S = 1/sL_s$, $Y_L = 1/sL_2$, $Y_C = sC$, and $Y_{CF} = sC_F$ are the admittances of grid reactance, inverter-side reactance, LCL filter capacitor, and compensation capacitor, respectively. The preceding admittance matrix is used to analyze parallel resonance. In addition, the impedance matrix should be obtained to analyze series resonance.

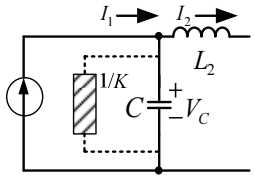

Fig. 3. Closed-loop simple circuit of a single-inverter system.

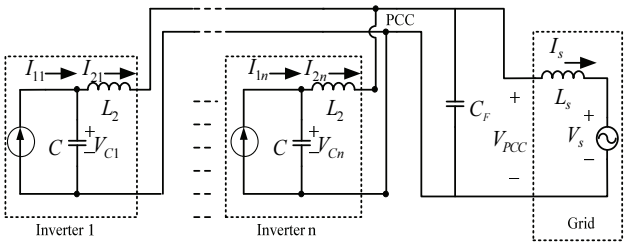

Fig. 4. Illustration of the proposed closed-loop model of multiple inverters.

From Eq. (8) and Table I, the eigenvalue matrix and the modal impedance can be obtained, and then the modal analysis map can be plotted to study resonant characteristics. The modal analysis results of a multi-inverter grid-connected system that contains a compensation capacitor without active damping are presented in Figs. 5 and 6, and the parameters of modal analysis are listed in Table I.

Fig. 5 illustrates the resonance features of a multi-inverter grid-connected system with several parallel inverters and compensation capacitors. When only one inverter is connected to the PCC, only one fixed resonance peak exists, whereas when several inverters are parallel with a compensation capacitor C_F, the system has three resonance peaks. The first resonance frequency is fixed. The second resonance frequency shifts to the left along the low-frequency region according to the number of parallel inverters. The third resonance frequency is located at the right of the fixed resonance peak, which is caused by the compensation capacitor, and moves toward the high-frequency region along with the number of parallel inverters. The third resonance frequency is near the switching frequency of certain equipment. The 5th and 7th harmonic currents are widespread in grid systems. Thus, the resonance caused by parallel multiple inverters can be easily justified.

The series resonances in a multi-inverter grid-connected system can be excited by grid voltage. Moreover, frequency depends on the number of parallel inverters as shown in Fig. 6. The two distinct resonances are the result of the interaction between parallel inverters and the compensation capacitor. These resonances are similar to the second and third types of parallel resonance, which may occur when grid voltage contains harmonics. Fig. 7 shows the modal analysis map

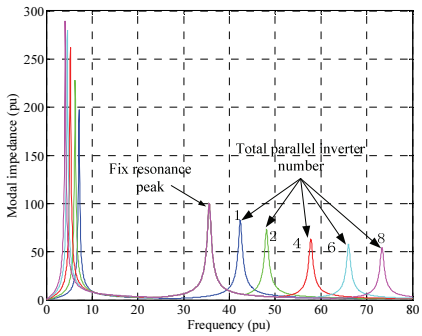

Fig. 5. Parallel resonance without active damping.

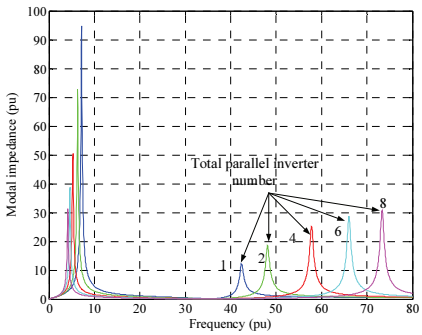

Fig. 6. Series resonance without active damping.

with different grid reactance L_S values. The fixed-frequency resonance peak is unaffected by grid reactance L_S. The second resonance frequency is at the left of the fixed resonance peak and is caused by parallel multiple inverters. The third resonance frequency is at the right of the fixed resonance peak, which is caused by the compensation capacitor. The second and third resonances move toward the high-frequency region with a decrease in grid reactance L_S. The amplitude of the two resonances decreases with a decrease in grid reactance L_S. The influence of filter capacitor C is shown in Fig. 8. When capacitance is high, the frequency of the resonance peak is low.

The compensation capacitor C_F at the grid side also affects resonance frequency. As shown in Fig. 9, the fixed-frequency resonance peak is unrelated to the C_F value. However, the second and third resonance peaks caused by C_F move to the high-frequency region with a decrease in compensation capacitor value.

From Figs. 5 to 9, the modal analysis map indicates that parallel inverters can introduce multiple resonances at different frequencies. These resonances may further excite grid current harmonics during transient and steady states. In addition, grid voltage includes background harmonics and transient disturbances; hence, series resonance can be excited. Therefore, grid current quality will be severely distorted without effective damping because of the existence of resonance.

When active damping-based virtual resistance is applied to the grid-connected inverter, the capacitor C of the LCL filter is equivalently paralleled with a resistance, whose value is $1/K$ ($K = 0.2$) at the resonance frequency. From the comparison

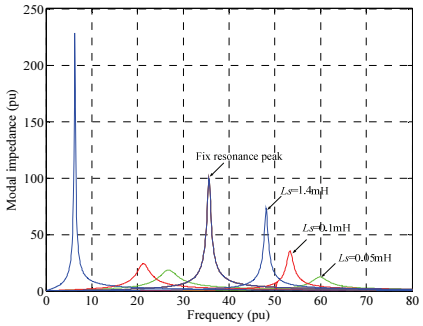

Fig. 7. Parallel resonance of a two-inverter system with different grid reactance L_S values (without active damping).

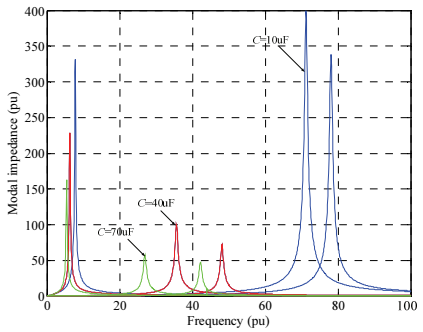

Fig. 8. Parallel resonance of a two-inverter system with different LCL filter capacitors C (without active damping).

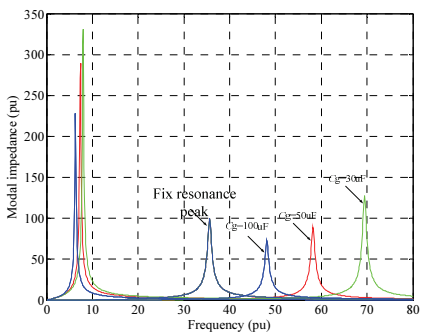

Fig. 9. Parallel resonance of a two-inverter system with different grid side compensation capacitors C_F (without active damping).

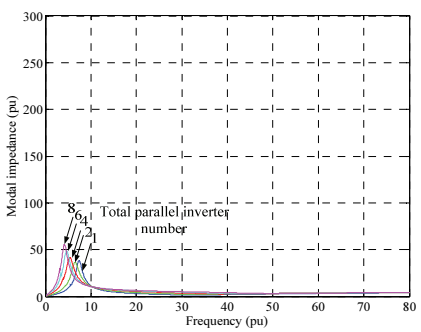

Fig. 10. Parallel resonance of a multi-inverter system (with active damping).

of Figs. 5 and 6, the effectiveness of active damping in multi-inverter system resonance suppression is also verified via modal analysis, as shown in Figs. 10 and 11. Through the

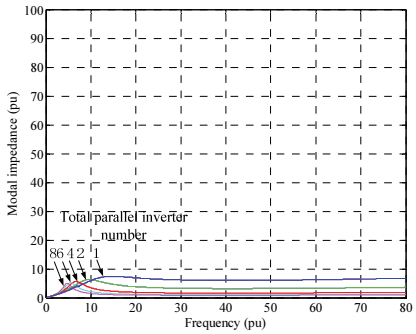

Fig. 11. Series resonance of a multi-inverter system (with active damping).

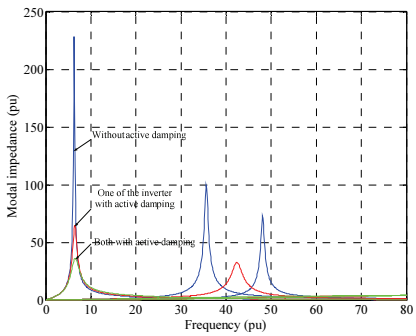

Fig. 12. Parallel resonance of a two-inverter system (with only one inverter using active damping).

selection of an appropriate virtual damping ratio, active damping based on virtual resistance is effective in restraining three types of resonance, namely, the fixed resonance caused by the LCL filter, the varying resonance caused by multiple inverters, and the resonance caused by the compensation capacitor. Only one inverter uses active damping; thus, the modal analysis map is suppressed as shown in Fig. 12. The resonance peak is weakened, but it still exists.

III. Discrete Domain Stability Analysis of Parallel Virtual Damping

The control factor K must be increased to obtain a higher damping ratio of parallel virtual resistance. However, high K values may impair system stability.

With the model shown in Fig. 4, the line current of inverter 1 can be obtained by applying Kirchoff's law as follows:

$$V_{\mathrm{PCC}}(z)=\frac{\left(\sum_{i=1}^{N} G_i(z)\cdot I_{\mathrm{ref},i}(z)+V_s(z)\cdot[Y_s(z)+Y_{CF}(z)]\right)}{\sum_{i=1}^{N} Y_{\mathrm{eq},i}(z)+Y_s(z)+Y_{CF}(z)}, \quad (9)$$

$$I_2(z)=G_1(z)I_{ref\,1}(z)-V_{PCC}(z)Y_{eq,1}(z) \quad , \quad (10)$$

where $G_1(z)$–$G_N(z)$ are the closed-loop transfer functions of the inverter line current, and $Y_{eq,1}(z)$–$Y_{eq,N}(z)$ are their associated admittances. $V_{\mathrm{pcc}}(z)$ is the voltage of PCC, $I_{\mathrm{ref},i}(z)$ is the current reference of the i-th inverter, $V_s(z)$ is the grid voltage, $Y_s(z)$ is the grid admittance, and $Y_{\mathrm{CF}}(z)$ is the admittance of the compensation capacitor.

From Eqs. (9) and (10), the line current of inverter 1 can be

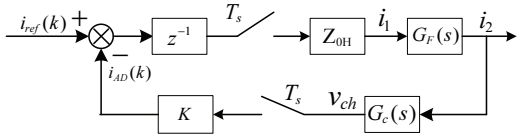

Fig. 13. Discrete current closed-loop control.

expressed as

$$I_2(z)=\overbrace{R_1(z)\cdot I_{\mathrm{ref}1}(z)}^{\text{Internal Resonance}}+\overbrace{\sum_{t=2}^{N} P_{1,t}(z)\cdot I_{\mathrm{ref},t}(z)}^{\text{Parallel Resonance}}-\overbrace{S_{G,1}(z)\cdot V_s(z)}^{\text{Series Resonance}} \quad (11)$$

The elements of Eq. (11) are given as

$$R_1(z)=G_1(z)\left\{1-\frac{Y_{\mathrm{eq},1}(z)}{\sum_{i=1}^{N} Y_{\mathrm{eq},i}(z)+Y_s(z)+Y_{CF}(z)}\right\};$$

$$P_{1,t}(z)=\frac{-Y_{\mathrm{eq},1}(z)\cdot G_t(z)}{\sum_{i=1}^{N} Y_{\mathrm{eq},i}(z)+Y_s(z)+Y_{CF}(z)}, \quad t\in[2,N];$$

$$S_{G,1}(z)=\frac{Y_{\mathrm{eq},1}(z)\cdot[Y_s(z)+Y_{CF}(z)]}{\sum_{i=1}^{N} Y_{\mathrm{eq},i}(z)+Y_s(z)+Y_{CF}(z)}.$$

Eq. (11) has three independent terms, and each term represents one type of resonance in a multi-inverter grid-connected system. To simplify the analysis, this section analyzes the stable domain of K using $G_1(z)$ as the study object.

The scheme of the control loop strategy for the inverter-side current is shown in Fig. 13, where $i_{ref}(k)$ is the reference current, $i_{AD}(k)$ is the damping current, T_s is the sampling cycle, and Z_{0H} is the zero-order holder. $G_F(s)$ is the transfer function of the LCL filter, which contains unstable poles. Without virtual damping control, the system is an open loop and unstable. The system can be turned into a stable closed-loop system by sampling capacitor harmonic voltage v_{ch} and selecting the appropriate value of K.

The transfer functions in Fig. 13 are

$$Z_{0H}(s)=\frac{1-e^{-Ts}}{s}, \quad (12)$$

$$G_F(s)=\frac{i_2(s)}{i_1(s)}=\frac{1}{s^2L_3C+1}=\frac{\omega_r^2}{s^2+\omega_r^2}, \quad (13)$$

$$G_c(s)=\frac{v_{ch}(s)}{i_2(s)}=\frac{i_c(s)}{i_2(s)}\times\frac{v_{ch}(s)}{i_c(s)}=s^2L_3C\times\frac{1}{sC}=sL_3, \quad (14)$$

where $L_3=L_2+L_s$. In Eq. (14), the influence of grid voltage is considered a disturbance.

The z-domain closed-loop transfer functions of the LCL filter is obtained as

$$G_1(z)=\frac{i_2(z)}{i_{ref}(z)}=\frac{z^{-1}\cdot Z(Z_{0H}\cdot G_F)}{1+z^{-1}\cdot K\cdot Z(Z_{0H}\cdot G_F\cdot G_c)}. \quad (15)$$

The z-domain closed-loop transfer functions can be obtained as

$$G_1(z)=\frac{(1-\cos\omega_rT_s)(z+1)}{z^3-2z^2\cos\omega_rT_s+(1+\omega_rL_3K\sin\omega_rT_s)z-\omega_rL_3K\sin\omega_rT_s}. \quad (16)$$

In accordance with Jury's stability criterion, when the third-order characteristic polynomial is expressed as $D(z)=a_0z^3$

$+a_1z^2+a_2z+a^3$, the necessary and sufficient condition for the stability of the system are (i) $|a_3|<|a_0|$, (ii) $D(1)>0$, (iii) $D(-1)<0$, and (iv) $|b_2|>|b_0|$,

where $b_0=\begin{vmatrix} a_3 & a_2 \\ a_0 & a_1 \end{vmatrix}, b_2=\begin{vmatrix} a_3 & a_0 \\ a_0 & a_3 \end{vmatrix}$.

From (i),

$$0<K<\frac{1}{\omega_r L_3 \sin(\omega_r T_s)} \quad . \tag{17}$$

From (ii), we can obtain

$$D(1)=2(1-\cos\omega_r T_s)>0 \cdot \tag{18}$$

From criterion (iii), we have

$$D(-1)=-2(1+\sqrt{1+(\omega_r L_3 K)^2}\sin(\omega_r T_s+\varphi))<0 \text{ ,} \tag{19}$$

where $tan\varphi = 1/\omega_r L_3 K$.

In accordance with Shannon's theorem, the actual sampling frequency must be greater than $5\omega_r$ to obtain virtual damping control given system resonant frequency ω_r. Therefore, Eqs. (20)–(22) can be obtained as follows:

$$0<\omega_r T_s<\pi/2 \quad , \tag{20}$$

$$0<\omega_r T_s+\varphi<\pi \quad , \tag{21}$$

$$\sin(\omega T_s+\varphi)>0>-1/\sqrt{1+(\omega L_3 K)^2} \quad . \tag{22}$$

The assumed conditions of criterion (iii) is expressed as

$$\omega_r<\frac{1}{T_s}\&K>0 \cdot \tag{23}$$

When criterion (iv) is considered,

$$|b_0|=|\omega_r L_3 K\sin(\omega_r T_s)(2\cos(\omega_r T_s)-1)-1| \text{ ,} \tag{24}$$

$$|b_2|=|(\omega_r L_3 K\sin(\omega_r T_s))^2-1| \cdot \tag{25}$$

When $|b_0|>1$ ($\omega_r T_s \geq \pi/3$), criterion (iv) will not be satisfied and the system will be unstable. When $\omega_r T_s<\pi/3$ is considered and by solving inequality $|b_2|>|b_0|$, we have

$$0<K<\frac{2ctg(\omega_r T_s)-\csc(\omega_r T_s)}{\omega_r L_3} \quad . \tag{26}$$

When $\omega_r T_s<\pi/3$ is considered and compared with criterion (i), we have

$$\frac{1}{\omega_r L_3\sin(\omega_r T_s)}\geq\frac{2\cos(\omega_r T_s)-1}{\omega_r L_3\sin(\omega_r T_s)}=\frac{2ctg(\omega_r T_s)-\csc(\omega_r T_s)}{\omega_r L_3} \quad . \tag{27}$$

The necessary and sufficient conditions for the stability of the system can be obtained as follows by integrating the four criteria:

$$(\omega_r T_s<\frac{\pi}{3})\ \&\ \&(0<K<\frac{2ctg(\omega_r T_s)-\csc(\omega_r T_s)}{\omega_r L_3}) \quad . \tag{28}$$

From Eq. (28), the curve of the maximum stable value of K versus the resonant frequency ω_r is shown in Fig. 14, and the inverter parameters are presented in Table I. When resonant frequency is high, the maximum stable value of K is low. This finding indicates that when the sampling frequency is fixed and the value of K increases, the corresponding resonant frequency decreases. Meanwhile, when the resonant frequency is fixed, a higher sampling frequency can improve stability.

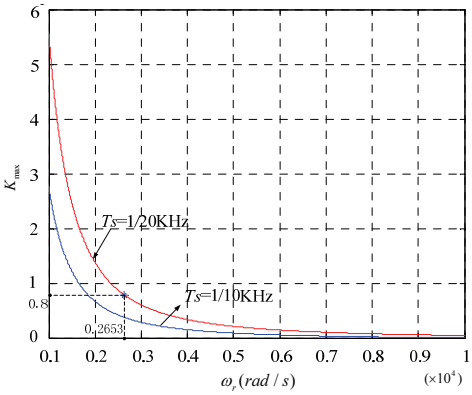

Fig. 14. Change rule of K_{max}.

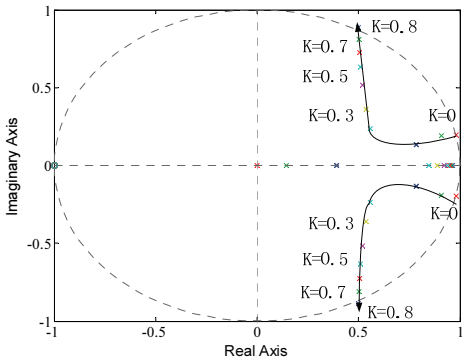

Fig. 15. Pole-zero maps with different active damping ratios (ω_r = 2635 rad/s).

Fig. 15 shows pole-zero maps that are obtained by selecting different K values. When K = 0 (no damping), two poles are outside the unit circle and the system is unstable. If K increases, then the unstable poles drop within the unit circle and the system becomes stable. However, two poles will go beyond the unit circle when K > 0.8, thereby making the system unstable again. The correctness of Eq. (28) is confirmed.

The proposed concept is verified on the MATLAB/Simulink platform. The multi-inverter grid-connected system shown in Fig. 1 is studied. The main parameters of the simulation system are provided in Table I.

Figs. 16 and 17 present the suppression effect of parallel resonance. The total simulation time is set as 0.4 s. Before 0.24 s, the value of K is zero and the system has no damping. The current contains harmonics. The resonance frequency of the single inverter is 7th, but resonance frequency varies from 7th to 5th after two inverters are connected in parallel. At 0.24 s, active damping is added to the system and K = 0.2. The quality of the current is improved. After 0.34 s, the value of K is outside the stability region. The output current is oscillating violently with K = 2.

Figs. 18 and 19 show the suppression effect of series

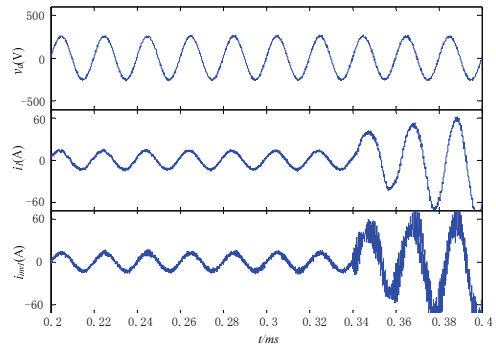

Fig. 16. Mitigation of single-inverter parallel resonance.

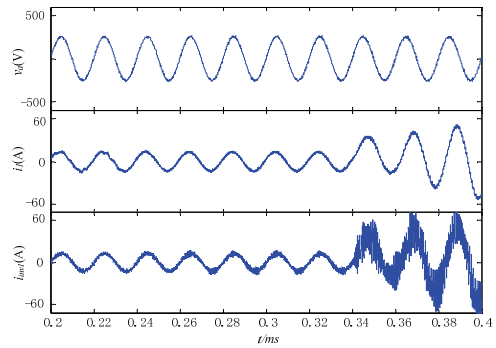

Fig. 17. Mitigation of two-inverter parallel resonance.

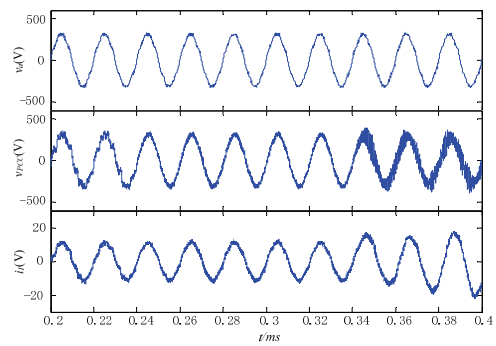

Fig. 18. Series resonance mitigation of a single inverter.

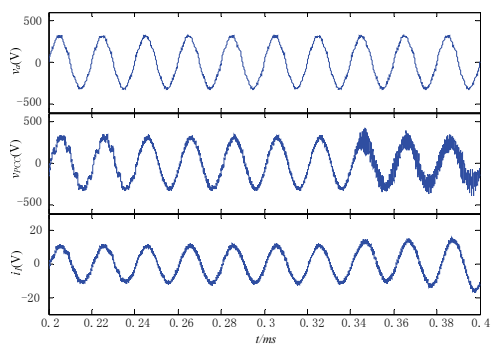

Fig. 19. Series resonance mitigation of two inverters.

resonance. The grid voltage contains 3% 5th and 3% 7th harmonic voltages. Before 0.24 s, the value of K is zero and the system has no damping. The voltage and current contain harmonics at PCC. The resonance frequency of the single inverter is 7th, but the resonance frequency varies from 7th to 5th after two inverters are connected in parallel. At 0.24 s, active damping is added to the system and K = 0.2. The qualities of current and voltage are improved at PCC. After 0.34 s, the value of K is outside the stability region with K = 2, and the current and voltage are oscillating violently at PCC.

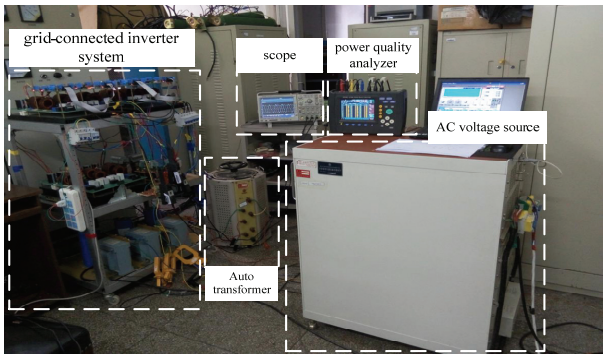

Fig. 20. Setup of the experiment system.

TABLE I
SYSTEM PARAMETERS

Description	Symbols	Value
Inverter side reactance	L_1	3.5 mH
Filter capacitor	C	40 μF
Grid side reactance	L_2	0.2 mH
Grid reactance	L_s	3.4 mH
Grid voltage	V_s	220 V/50 Hz
DC bus voltage	V_{dc}	700 V
Sampling frequency	f_s	20 kHz
Capacitor	C_F	100 μF
Resonant frequency	ω_r	2635 rad/s

IV. EXPERIMENT VERIFICATION

The proposed modal analysis and stability domain calculation of active damping are verified via experiments on a scaled-down laboratory prototype, the circuit of which is the same as that of the simulation shown in Fig. 1. The setup of the experiment system is shown in Fig. 20. The system parameters are listed in Table I. The experimental multi-inverter grid-connected system consists of two three-phase inverters supplied by a standard three-phase rectifier. No DC voltage loop is used. The digital controllers consist of a digital signal processor (TMS320F28335) and a complex programmable logic device (EPM570T100).

The performance of a single inverter that uses active damping with different values of K is shown in Figs. 21 and 22. When conventional control without damping (K = 0) is implemented, line current has some steady-state harmonics. After the active damping scheme is enabled (K = 0.2), the quality of line current is improved. However, once the active

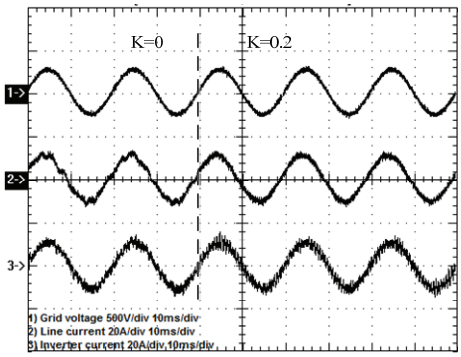

Fig. 21. Performance of a single inverter with active damping. (1) Grid voltage: 500 V/div. (2) Line current of inverter 1: 20 A/div. (3) Inverter 1 current: 20 A/div.

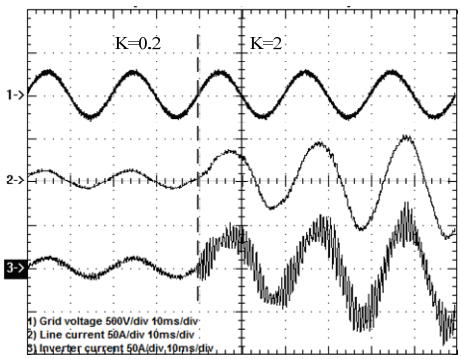

Fig. 22. Performance of a single inverter with different active damping ratios. (1) Grid voltage: 500 V/div. (2) Line current of inverter 1: 50 A/div. (3) Inverter 1 current: 50 A/div.

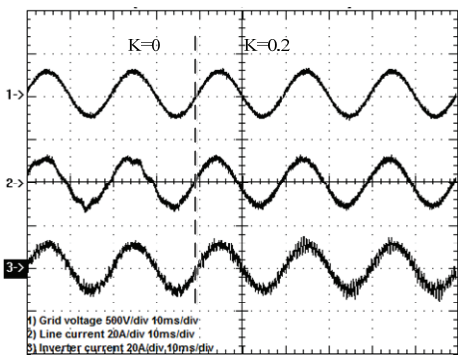

Fig. 23. Mitigation of two-inverter parallel resonance with active damping. (1) Grid voltage: 500 V/div. (2) Line current of inverter 1: 20 A/div. (3) Inverter 1 current: 20 A/div.

damping ratio K is beyond the stable area (K = 2), drastic oscillation of the inverter and line currents will occur.

To investigate parallel resonance, two inverters are connected to PCC. The active damping ratio K has two step changes: from 0 to 0.2 and from 0.2 to 2. The line currents are shown in Figs. 23 and 24. As illustrated, the line currents of both inverters are distorted without active damping, and the dominant resonance changes from 7th harmonics to 5th harmonics due to the operation of inverter 2. Similar to that in Figs. 21 and 22, when active damping ratio K is in the stable region, better line current quality can be obtained, thereby reducing parallel resonance peak.

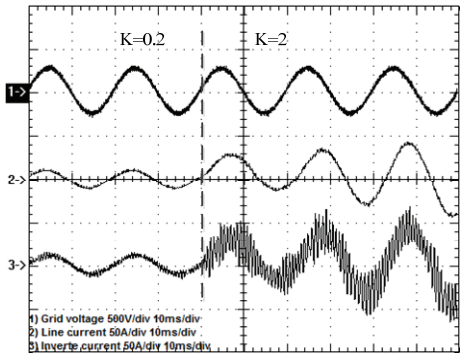

Fig. 24. Mitigation of two-inverter parallel resonance with different active damping ratios. (1) Grid voltage: 500 V/div. (2) Line current of inverter 1: 50 A/div. (3) Inverter 1 current: 50 A/div.

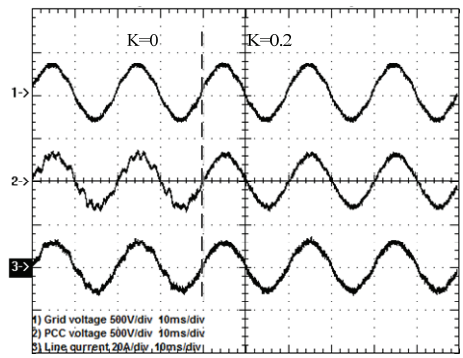

Fig. 25. Series resonance mitigation of a single inverter with active damping. (1) Grid voltage: 500 V/div. (2) PCC voltage: 500 V/div. (3) Line current of inverter 1: 20 A/div.

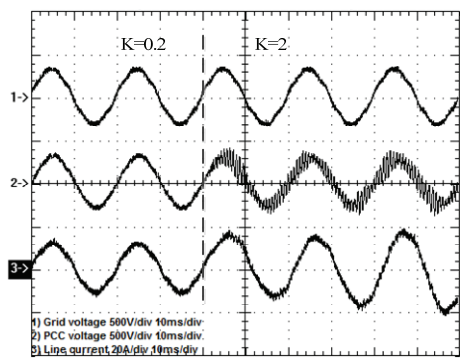

Fig. 26. Series resonance mitigation of a single inverter with different active damping ratios. (1) Grid voltage: 500 V/div. (2) PCC voltage: 500 V/div. (3) Line current of inverter 1: 20 A/div.

The steady-state series resonances in a multi-inverter grid-connected system are tested. Grid voltage is emulated by a programmable voltage source that contains 3% 5th and 3% 7th steady-state harmonics. When only a single inverter is operating, the performance of active damping with different K values is shown in Figs. 25 and 26. The line current of inverter 1 and PCC voltage are severely deteriorated by the series resonance between the multi-inverter and the grid. In addition, the major harmonic is the 7th harmonic. With the active damping method, the steady-state power quality of PCC voltage and line current can be significantly improved.

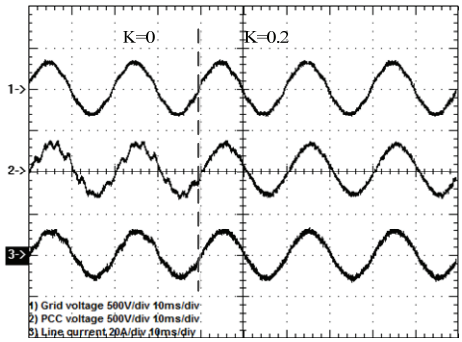

Fig. 27. Series resonance mitigation of two inverters with active damping. (1) Grid voltage: 500 V/div. (2) PCC voltage: 500 V/div. (3) Line current of inverter 1: 20 A/div.

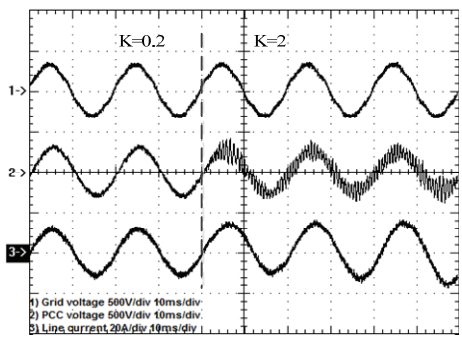

Fig. 28. Series resonance mitigation of two inverters with different active damping ratios. (1) Grid voltage: 500 V/div. (2) PCC voltage: 500 V /div. (3) Line current of inverter 1: 20 A/div.

Meanwhile, when two inverters are used, the dominant resonance in PCC voltage and line current changes from 7^{th} harmonics to 5^{th} harmonics due to the operation of inverter 2, as shown in Figs. 27 and 28. Therefore, steady-state harmonics will change in a distributed system with variable inverter numbers. When active damping is used and the ratio K is in the stable region, series resonance can be restrained and better PCC voltage and line current qualities are obtained.

V. CONCLUSIONS

In this paper, the interaction among the grid, capacitance, and multiple grid-connected inverters is discussed with the support of analyses and experiments. This paper describes a simple model that uses a deadbeat current-controlled voltage source inverter. The inverter-side reactor does not need to be considered, and the complexity of analysis can be reduced. This study shows that the multi-inverter grid-connected system has more complex resonances in the presence of compensation capacitors in a distribution power system. To identify resonance frequency, this study develops a modal analysis method based on the proposed simple model. In addition, the stability of active damping based on virtual resistance is analyzed in the discrete domain, and the relationship among sampling frequency, active damping ratio, and system parameters is presented. The simulation and experimental results demonstrate the effectiveness of the proposed analysis.

ACKNOWLEDGMENT

This paper and its related research are supported by grants from the National Natural Science Foundation of China (51407043) and the National High Technology Research and Development Program 863 of China (2015AA050603).

REFERENCES

[1] L. Wang, H. Gao, and G. Zou, "Modeling methodology and fault simulation of distribution networks integrated with inverter-based DG," *Protection and Control of Modern Power Systems*, Vol. 2, No. 31, pp. 1-9, Aug. 2017.

[2] W. Guo and L. Mu, "Control principles of micro-source inverters used in microgrid," *Protection and Control of Modern Power Systems*, Vol. 1, No. 5, pp. 1-7, Jun. 2016.

[3] J. M. Carrasco, L. G. Franquelo, J. T. Bialasiewwicz, E. Galvan, R. C.P. Guisado, M. A. M. Prats, J. I. Leon, and N. Moreno-Alfonso, "Power electronic systems for the grid integration of renewable energy sources: A survey," *IEEE Trans. Ind. Electron*., Vol. 53, No. 4, pp. 1002-1016, Jun. 2006.

[4] M. H. Bierhoff and F. W. Fuchs, "Active damping for three-phase PWM rectifiers with high-order line-side filters," *IEEE Trans. Ind. Electron*., Vol. 56, No. 2, pp. 371-379, Feb. 2009.

[5] E. Wu and P. W. Lehn, "Digital current control of a voltage source converter with active damping of LCL resonance," *IEEE Trans. Power Electron*., Vol. 21, No. 5, pp. 1364-1373, Sep. 2006.

[6] J. Dannehl, F. W. Fuchs, S. Hansen, and P. B. Thogersen, "Investigation of active damping approaches for PI-based current control of grid-connected pulse width modulation converters with LCL filters," *IEEE Trans. Ind. Applicat*., Vol. 46, No. 4, pp. 1509-1517, Jul./Aug. 2010.

[7] J. R. Massing, M. Stefanello, H. A. Grundling, and H. Pinheiro, "Adaptive current control for grid-connected converters with LCL filter," *IEEE Trans. Ind. Electron*., Vol. 59, No. 12, pp.4681-4693, Dec. 2012.

[8] J. H. R. Enslin and P. J. M. Heskes, "Harmonic interaction between a large number of distributed power inverters and the distributed network," *IEEE Trans. Power Electron*., Vol. 19, No. 6, pp. 1586-1593, Nov. 2004.

[9] J. L. Agorreta, M. Borrega, J. Lopez, and L. Marroyo, "Modeling and control of N-paralleled grid-connected inverters with LCL filters coupled due to grid impedance in PV plants," *IEEE Trans. Ind. Electron*., Vol. 26, No. 3, pp. 770-785, Mar. 2011.

[10] F. Wang, J. L. Duarte, M. A. M. Hendrix, and P. F. Ribeiro, "Modeling and analysis of grid harmonic distortion impact of aggregated DG inverters," *IEEE Trans. Power Electron*., Vol. 26, No. 3, pp.786-797, Mar. 2011.

[11] X. Wang, F. Blaabjerg, and W. Wu, "Modeling and analysis of harmonic stability in an AC power-electronics-based power system," *IEEE Trans. Power Electron*., Vol. 29, No. 12, pp. 6421-6432, Dec. 2014.

[12] J. He, Y. Li, D. Bosnjak, and B. Harris, "Investigation and active damping of multiple resonances in a parallel-inverter-based microgrid," *IEEE Trans. Power Electron*., Vol. 28, No. 1, pp. 234-246, Jan. 2013.

[13] Q. N. Trinh and H. H. Lee, "An advanced current control strategy for three-phase shunt active power filters," *IEEE Trans. Ind. Electron*., Vol. 60, No. 12, pp. 5400-5410, Dec. 2013.
[14] N. Prabhakar and M. K. Mishra, "Dynamic hysteresis current control to minimize switching for three-phase four-Leg VSI topology to compensate nonlinear load," *IEEE Trans. Power Electron*., Vol. 25, No. 8, pp.1935-1942, Aug. 2010.
[15] F. Wu, B. Sun, K. Zhao, and L. Sun, "Analysis and solution of current zero-crossing distortion with unipolar deadbeat current control in grid-connected inverter," *IEEE Trans. Ind. Electron*., Vol. 60, No. 10, pp. 4450-4457, Oct. 2013.
[16] Y. Cui and W. Xu, "Harmonic resonance mode analysis using real symmetrical nodal matrices," *IEEE Trans. Power Del*., Vol. 22, No. 3, pp.1989-1990, Jul. 2007.
[17] Z. Huang, Y. Cui, and W. Xu, "Application of modal sensitivity for power system harmonic resonance analysis," *IEEE Trans. Power Del*., Vol. 22, No. 1, pp. 222-231, Jan. 2011.
[18] Y. Cui and X. Wang, "Modal frequency sensitivity for power system harmonic resonance analysis," *IEEE Trans. Power Del*., Vol. 27, No. 2, pp.1010-1017, Apr. 2012.

Jian Wu was born in Harbin, China in 1979. He obtained his B.S., M.S., and Ph.D. in Electrical Engineering from Harbin Institute of Technology (HIT), Harbin, China, in 2001, 2003, and 2007, respectively. He joined the Department of Electrical Engineering, HIT as a lecturer in 2007. His research interests include power quality, voltage source converter high-voltage direct current, monitoring schemes for distribution networks, and multi-level converters.

Tao Chen was born in Chongqing, China in 1994. He obtained his B.S. degree from Harbin Institute of Technology, Harbin, China in 2017, where he is currently working for an M.S. degree in the School of Electrical Engineering and Automation. His current research interests include high-power electronics, multilevel converters, and DC/DC converters.

Wanqin Han was born in Chongqing, China in 1994. She obtained her B.S. degree from the Harbin Institute of Technology, Harbin, China in 2017, where she is currently working for an M.S. degree in the School of Electrical Engineering and Automation. Her current research interests include high-power electronics, multilevel converters, and DC/DC converters.

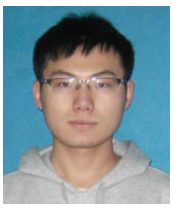

Jiaqi Zhao was born in Chongqing, China in 1994. She obtained her B.S. degree from the Harbin Institute of Technology, Harbin, China in 2016, where she is currently working for an M.S. degree in the School of Electrical Engineering and Automation. His current research interests include high-power electronics, multilevel converters, and DC/DC converters.

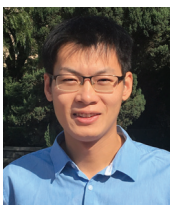

Binbin Li obtained his B.S., M.S., and Ph.D. in Electrical Engineering from Harbin Institute of Technology (HIT), Harbin, China in 2010, 2012, and 2017, respectively. From November 2015 to November 2016, he was a visiting researcher in the Department of Electronic and Electrical Engineering, University of Strathclyde, Glasgow, U.K. He is currently an associate professor in the Department of Electrical Engineering, HIT. His research interests include multilevel converters, high-power electronics, control algorithms, and pulse-width modulation techniques.

Dianguo Xu obtained his B.S. in Control Engineering from Harbin Engineering University, Harbin, China, in 1982, and his M.S. and Ph.D.in Electrical Engineering from Harbin Institute of Technology (HIT), Harbin, China in 1984 and 1989, respectively. He joined the Department of Electrical Engineering, HIT as an assistant professor in 1984. He has been a professor in the Department of Electrical Engineering, HIT since 1994. He was the dean of the School of Electrical Engineering and Automation, HIT from 2000 to 2010. He is currently the vice president of HIT. His research interests include renewable energy generation technology, multiterminal HVDC systems based on VSCs, power quality mitigation, speed sensorless vector-controlled motor drives, and high-performance PMSM servo systems. He has published over 600 technical papers. Prof. Xu is an associate editor of the IEEE Transactions on Industrial Electronics and the IEEE Journal of Emerging and Selected Topics in Power Electronics. He is also serving as the chairman of the IEEE Harbin Section, the director of the Lighting Power Supply Committee of CPSS, and the vice director of the Electric Automation Committee of CAA, the Electrical Control System and Equipment Committee of CES, and the Power Electronics Committee of CES.